

Upcrossing-rate dynamics for a minimal neuron model receiving spatially distributed synaptic drive

Robert P. Gowers^{1,2,3} and Magnus J. E. Richardson^{1,*}

¹Warwick Mathematics Institute, University of Warwick, CV4 7AL, United Kingdom

²Institute for Theoretical Biology, Humboldt-Universität zu Berlin, 10115 Berlin, Germany

³Bernstein Center for Computational Neuroscience, 10115 Berlin, Germany



(Received 3 October 2022; revised 3 October 2022; accepted 2 March 2023; published 12 May 2023)

This article is part of the Physical Review Research collection titled *Physics of Neuroscience*.

The spatiotemporal stochastic dynamics of the voltage, as well as the upcrossing rate, are derived for a model neuron comprising a long dendrite with uniformly distributed filtered excitatory and inhibitory synaptic drive. A cascade of ordinary and partial differential equations is obtained describing the evolution of first-order means and second-order spatial covariances of the voltage and its rate of change. These quantities provide an analytical form for the general, steady-state, and linear response of the upcrossing rate to dynamic synaptic input. It is demonstrated that this minimal dendritic model has an unexpectedly sustained high-frequency response despite synaptic, membrane, and spatial filtering.

DOI: [10.1103/PhysRevResearch.5.023095](https://doi.org/10.1103/PhysRevResearch.5.023095)

I. INTRODUCTION

Neurons are spatially extended cells receiving a high density of synapses on their dendrites [1] and can be modeled as threshold devices that integrate filtered stochastic input from presynaptic populations. Over the last few decades there have been significant advances in the mathematical analysis of neuronal input-output functions, typically in an approximation in which the cell is treated as isopotential [2]. Simultaneously, there has been growing interest in how spatially induced voltage differences throughout the dendritic arbour might support computational capacities beyond the isopotential approximation. These latter studies have been overwhelmingly simulational [3] due to the difficulty in accounting for spatial structure and nonlinear filtering.

There is a relative sparsity of results for stochastic synaptic integration in neurons with explicit spatial structure [4–9]. However, earlier studies of isopotential neurons demonstrate that analytical statements derived from reduced models provide a general and enduring framework that are an important guide for biophysically detailed but particular simulational studies. With this in mind, here a minimal model of spatiotemporal integration is considered and solved for both the stochastic voltage and firing-rate dynamics.

We first derive a set of partial differential equations that describe the spatiotemporal voltage fluctuations under dendritic integration of stochastic synaptic drive. We then adapt Rice's level-crossing approximation [10], widely used for isopotential models [11–18], to demonstrate that the high-frequency

response of the upcrossing rate exhibits a much weaker effect of the cascade of synaptic, membrane, and spatial filtering than might naively be expected.

II. MODEL

The voltage $V(x, t)$ of an infinite dendrite, with a threshold crossing V_{th} tested at $x = 0$ only, obeys

$$\partial_t V = \alpha_\ell(E_\ell - V) + H_e(E_e - V) + H_i(E_i - V) + D\partial_x^2 V, \quad (1)$$

where the leak and synaptic conductances per unit area have been divided by capacitance per unit area to give ratelike quantities α_ℓ , $H_s(x, t)$ and where E_ℓ , E_s are the associated reversal potentials. We will use the notation $s = e, i$ throughout to denote excitation or inhibition, respectively. The diffusive term of constant strength $D = \lambda_\ell^2 \alpha_\ell$, where λ_ℓ is the electrotonic length, captures the effect of axial-current flow through the dendritic core. Structurally, the model can be interpreted as a neuron with two long dendrites stemming from a small soma that has no additional conductance load.

The response to an isolated excitatory synaptic input $\tau_e \dot{H}_e + H_e \propto \delta(x)\delta(t)$, where τ_e is the excitatory synaptic time constant, is plotted in Figs. 1(a) and 1(b). In the latter panel the temporal profiles at different distances are compared to that of an isopotential model where $D = 0$ and $\tau_e \dot{H}_e + H_e \propto \delta(t)$. The time to peak for nearby input is shorter than for the isopotential model and so the cross-over behavior [see the inset of Fig. 1(b)] suggests that the minimal dendritic model might have a more rapid response to synaptic drive than the isopotential model, despite the additional spatial filtering.

To examine whether this is or is not the case, we developed a model of spatially distributed synaptic drive with the arrival of presynaptic spikes approximated as space-time Gaussian white-noise processes $\eta_s(x, t)$ filtered at physiological timescales $\tau_e = 3$ ms and $\tau_i = 10$ ms. Therefore,

$$\tau_s \dot{H}_s = \alpha_s - H_s + \sqrt{\alpha_s \lambda_s} \eta_s(x, t), \quad (2)$$

*Corresponding author: magnus.richardson@warwick.ac.uk

Published by the American Physical Society under the terms of the [Creative Commons Attribution 4.0 International](https://creativecommons.org/licenses/by/4.0/) license. Further distribution of this work must maintain attribution to the author(s) and the published article's title, journal citation, and DOI.

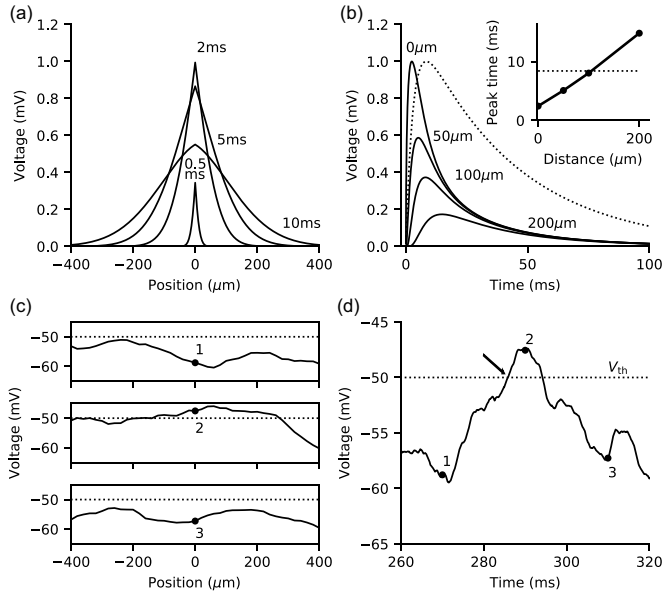


FIG. 1. Spatiotemporal voltage profiles for a single synaptic pulse (a) and (b), and widespread stochastic synaptic drive (c) and (d). (a) Spatial profiles for a synaptic pulse at the origin at times marked. (b) Temporal profiles at distances marked (corresponding isopotential neuron form, dotted line). Inset shows time-to-peak is shorter than the isopotential case (dotted line) for nearby inputs. (c) Spatial profiles of three snapshots separated by 20 ms during widespread stochastic synaptic input (threshold $V_{th} = -50$ mV, dotted line). (d) Temporal voltage profile at $x = 0$. Labeled symbols correspond to those in panel 1(c). An upcrossing event passing V_{th} from below is marked (arrow). Parameters used were $(E_\ell, E_e, E_i) = (-60, -80, 0)$ mV, $(\tau_e, \tau_i) = (3, 10)$ ms, $(\alpha_\ell, \alpha_e, \alpha_i) = (25, 5.6, 11)$ Hz, and $(\lambda_\ell, \lambda_e, \lambda_i) = (224, 19, 64)$ μ m. All simulations were written in Julia [19] with details provided in Appendix D and code in the Supplemental Material [31].

where $\alpha_s(t)$ is proportional to the presynaptic rate and λ_s a length constant. The zero-mean white noise has autocovariance $\langle \eta_s(x_1, t_1) \eta_s(x_2, t_2) \rangle = \delta(x_1 - x_2) \delta(t_1 - t_2)$. Excitation and inhibition are considered statistically uncorrelated, though this can be accommodated within the calculational framework to be presented. The model [Eqs. (1) and (2)] is closely related to Tuckwell's [6] but includes multiple synaptic timescales and dynamic conductances.

The voltage and synaptic state-variables are now resolved into deterministic (mean) and fluctuating (zero mean) components, for example $V(x, t) = \langle V \rangle(t) + v(x, t)$, where the deterministic parts are temporally dependent but spatially independent and obey

$$\begin{aligned} \partial_t \langle V \rangle &= \alpha_\ell (E_\ell - \langle V \rangle) + \langle H_e \rangle (E_e - \langle V \rangle) + \langle H_i \rangle (E_i - \langle V \rangle), \\ \tau_e \partial_t \langle H_e \rangle &= \alpha_e - \langle H_e \rangle, \text{ and } \tau_i \partial_t \langle H_i \rangle = \alpha_i - \langle H_i \rangle. \end{aligned} \quad (3)$$

The fluctuating components v , h_e , h_i are functions of space and time and obey the partial-differential equations

$$\begin{aligned} \partial_t v &= h_e \mathcal{E}_e + h_i \mathcal{E}_i - \mathcal{H}v + D \partial_x^2 v, \\ \tau_e \partial_t h_e &= \sqrt{\alpha_e \lambda_e} \eta_e - h_e, \text{ and } \tau_i \partial_t h_i = \sqrt{\alpha_i \lambda_i} \eta_i - h_i, \end{aligned} \quad (4)$$

where $\mathcal{E}_s(t) = (E_s - \langle V \rangle)$ and $\mathcal{H}(t) = \alpha_\ell + \langle H_e \rangle + \langle H_i \rangle$ are spatially independent, though generally time dependent. Note that in deriving Eqs. (3) and (4) we have dropped relatively less significant terms like $\langle v h_e \rangle$ [5,20] so the voltage has Gaussian statistics. Figures 1(c) and 1(d) provide examples of the spatiotemporal dynamics and an upcrossing event.

The upcrossing rate [10] is a nonlinear function of two first-order and three second-order voltage moments $r_{uc}(\langle V \rangle, \langle \dot{V} \rangle, \langle v^2 \rangle, \langle v \dot{v} \rangle, \langle \dot{v}^2 \rangle)$ with the full form provided in Appendix A. The first-order moments are given by Eqs. (3). To obtain the second-order moments we derive partial differential equations for the same-time space-separated covariances. Introducing the shorthand $\langle h_s^2 \rangle_x = \langle h_s(x_1, t) h_s(x_2, t) \rangle$, where $x = x_2 - x_1$, we first formally solve for the same-time synaptic autocovariance

$$\langle h_s^2 \rangle_x = \delta(x) \frac{\lambda_s}{\tau_s^2} \int_{-\infty}^t dt' e^{-2(t-t')/\tau_s} \alpha_s(t'). \quad (5)$$

This integral is also the solution of a linear partial-differential equation for $\langle h_s^2 \rangle_x$ [see Eq. (6)]. We can also derive partial-differential equations for other covariances by taking various moments of Eqs. (4) to give

$$\frac{\tau_s}{2} \partial_t \langle h_s^2 \rangle_x = \delta(x) \frac{\alpha_s \lambda_s}{2 \tau_s} - \langle h_s^2 \rangle_x, \quad (6)$$

$$\partial_t \langle v h_s \rangle_x = \mathcal{E}_s \langle h_s^2 \rangle_x - \left(\mathcal{H} + \frac{1}{\tau_s} \right) \langle v h_s \rangle_x + D \partial_x^2 \langle v h_s \rangle_x, \quad (7)$$

$$\frac{1}{2} \partial_t \langle v^2 \rangle_x = \mathcal{E}_e \langle v h_e \rangle_x + \mathcal{E}_i \langle v h_i \rangle_x - \mathcal{H} \langle v^2 \rangle_x + D \partial_x^2 \langle v^2 \rangle_x, \quad (8)$$

where we additionally have $\langle v \dot{v} \rangle_x = \partial_t \langle v^2 \rangle_x / 2$. For the autocovariance of \dot{v} we will need the relation

$$\langle \dot{v} h_s \rangle_x = \partial_t \langle v h_s \rangle_x + \langle v h_s \rangle_x / \tau_s \quad (9)$$

derived by multiplying the synaptic conductance Eq. (4) by v and taking moments while noting that $\langle v \eta_s \rangle = 0$ due to causality. The above relation is used for the autocovariance of the rate-of-change of voltage

$$\langle \dot{v}^2 \rangle_x = \mathcal{E}_e \langle \dot{v} h_e \rangle_x + \mathcal{E}_i \langle \dot{v} h_i \rangle_x - \mathcal{H} \langle v \dot{v} \rangle_x + D \partial_x^2 \langle v \dot{v} \rangle_x. \quad (10)$$

The covariance Eqs. (6)–(10), with $s = e, i$ provide a feedforward cascade allowing all momentlike quantities to be derived for the upcrossing dynamics by solving for the x and t dependence and then setting $x = 0$.

It should be noted that these equations are valid for arbitrary presynaptic rate dynamics and are not linear approximations. An example of the response to changes in the presynaptic rates comprising onset/offset and multiple frequency components is provided in Fig. 2. It can be seen that moments including \dot{V} or \dot{v} have sustained responses at higher frequencies.

III. STEADY-STATE PROPERTIES

Before calculating frequency-dependent properties, we first derive forms for the different spatial covariances and moments required for the steady-state upcrossing rate. The notation \bar{Q} is used for the steady-state value of a quantity $Q(t)$.

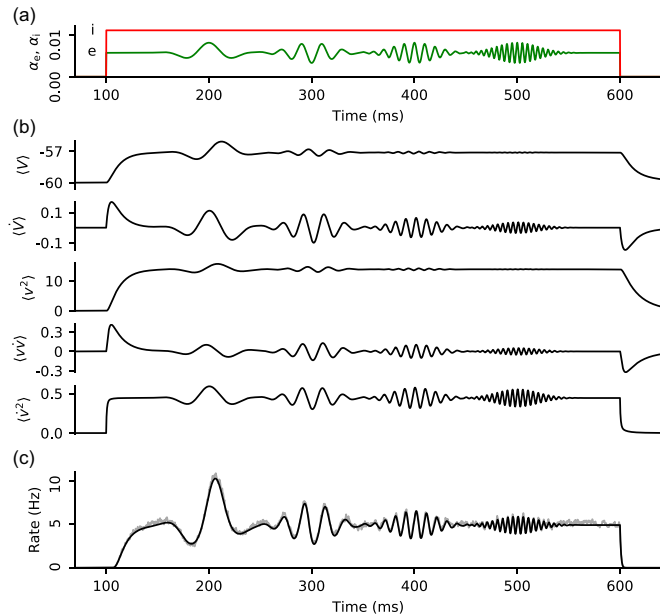


FIG. 2. Response to patterned synaptic input (a) comprising separate increases in excitatory (green) and inhibitory (red) drive [same parameters as Fig. 1(c)] with excitatory chirps at 20, 50, 100, 200 Hz. (b) First and second-order voltage moments with those containing a voltage derivative showing stronger responses at higher frequencies. (c). The upcrossing rate is a nonlinear function of the various moments (see Appendix A) and also shows a relatively sustained response at higher frequencies, despite the filtering from synapses, spatial spreading and the membrane time constant. The mathematical form of the patterned input is provided in Appendix D.

The steady-state means are calculated using $\langle \bar{H}_s \rangle = \bar{\alpha}_s$ for the two synaptic conductances. These give the steady-state average voltage as the standard weighted average of reversal potentials $\langle \bar{V} \rangle = (\alpha_\ell E_\ell + \bar{\alpha}_e E_e + \bar{\alpha}_i E_i) \tau_v$ where $1/\tau_v = \bar{H} =$

$\alpha_\ell + \bar{\alpha}_e + \bar{\alpha}_i$. For the steady-state fluctuating components, it proves convenient to introduce an effective space constant λ_v defined through $\lambda_v^2 = D\tau_v$. We note that the steady-state synaptic conductance fluctuations in Eq. (6) are delta correlated in space $\langle \bar{h}_s^2 \rangle_x = \delta(x) \bar{\alpha}_s / 2\tau_s$ and so when substituted into the steady-state version of Eq. (7) will provide a gradient condition on $\langle \bar{v} h_s \rangle_x$ at $x = 0$. Given $\psi = \psi_0 e^{-|x|/k}$ solves $\psi'' = k^2 \psi - 2k\delta(x)\psi_0$ we have

$$\langle \bar{v} h_s \rangle_x = \frac{\bar{\mathcal{E}}_s}{4\tau_s} \bar{\alpha}_s \tau_v \frac{\lambda_s}{\lambda_v} \sqrt{\frac{\tau_s}{\tau_v + \tau_s}} e^{-|x|/k_s}, \quad (11)$$

where $k_s^2 \lambda_v^2 = (\tau_v + \tau_s) / \tau_s$. An illustration for excitation and inhibition is provided in the upper panel of Fig. 3(a). The equation for the steady-state voltage autocovariance is separated into excitatory and inhibitory components $\langle \bar{v}^2 \rangle_x = \langle \bar{v}^2 \rangle_x^e + \langle \bar{v}^2 \rangle_x^i$ and solved similarly (see Appendix B);

$$\langle \bar{v}^2 \rangle_x^s = \frac{\bar{\mathcal{E}}_s^2}{4} \bar{\alpha}_s \tau_v \frac{\lambda_s}{\lambda_v} \left(e^{-|x|/k_v} - \sqrt{\frac{\tau_s}{\tau_v + \tau_s}} e^{-|x|/k_s} \right), \quad (12)$$

where $k_v = 1/\lambda_v$. Unlike the covariance between voltage and a synaptic drive, the voltage autocovariance has zero gradient at the origin [see the middle panel of Fig. 3(a)]. The final quantity needed for the steady-state upcrossing rate is the autocovariance of \dot{v} that takes the form $\langle \dot{v}^2 \rangle_x = \bar{\mathcal{E}}_e \langle \bar{v} h_e \rangle_x / \tau_e + \bar{\mathcal{E}}_i \langle \bar{v} h_i \rangle_x / \tau_i$. Each synaptic component of this quantity is easily expressed using the second of the two results in Eq. (11) and so

$$\langle \dot{v}^2 \rangle_x^s = \frac{\bar{\mathcal{E}}_s^2}{4\tau_s^2} \bar{\alpha}_s \tau_v \frac{\lambda_s}{\lambda_v} \sqrt{\frac{\tau_s}{\tau_s + \tau_v}} e^{-|x|/k_s} \quad (13)$$

with an illustration provided in the lower panel of Fig. 3(a). The result for $\langle \bar{V} \rangle$ and Eqs. (12) and (13) evaluated at $x = 0$ provide the quantities needed for the steady-state upcrossing rate [see Fig. 3(c)].

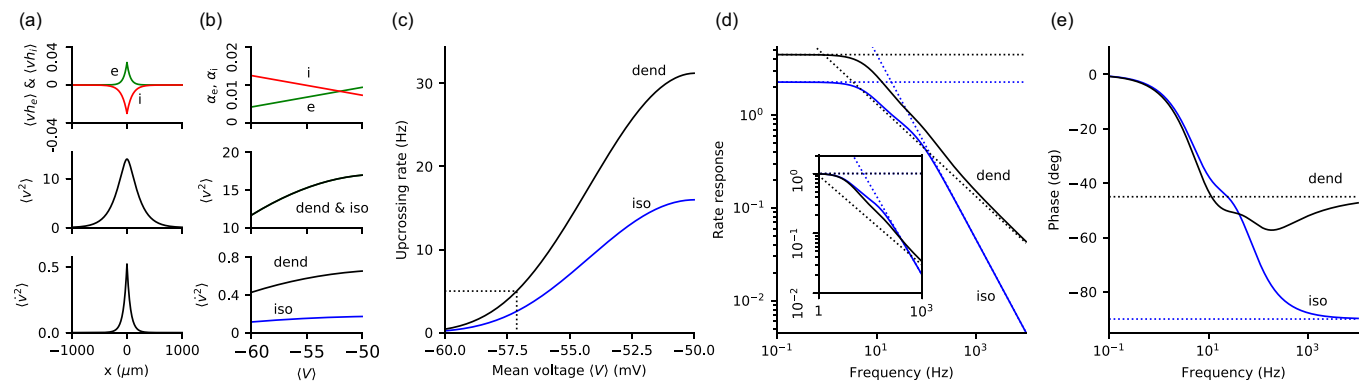


FIG. 3. Steady-state (a)–(c) and upcrossing-rate response (d) and (e) showing a weakly attenuated response at high frequencies. (a) Steady-state spatial covariances of synaptic and voltage variables. (b) Steady-state synaptic drive covaried to provide a particular mean voltage (x axis) at fixed conductance levels. For an isopotential neuron with matched voltage mean, variance, and conductance, a difference in the rate of change of voltage is seen (lower panel, blue). (c) Steady-state upcrossing rate as a function of mean voltage for the dendritic (black) and isopotential model (blue). (d) Upcrossing-rate response by frequency normalized by $\bar{\alpha}_e$. Note that the dendritic-model response shows qualitatively weaker attenuation at high-frequency $\sim 1/\sqrt{i\omega}$ than the reference isopotential model $\sim 1/i\omega$. Inset shows same curves normalized at zero frequency in which it is seen that the response of the dendritic and isopotential models are broadly similar even over moderate frequencies despite the additional spatial filtering. (e) Upcrossing phase as a function of frequency with a -45° asymptote for the dendritic case and -90° for the isopotential model. Parameters used are the same as Fig. 1.

IV. FIRING-RATE RESPONSE

We now derive the frequency-dependent response by considering weak sinusoidal modulations of the incoming excitatory synaptic rate $\alpha_e(t) = \bar{\alpha}_e + \hat{\alpha}_e e^{i\omega t}$ and expand all state variables to leading order in $\hat{\alpha}_e$. We will use the notation for some quantity $Q(t) = \bar{Q} + \hat{Q} e^{i\omega t}$ with \bar{Q} the steady-state value and \hat{Q} the linear response proportional to $\hat{\alpha}_e$. At this level, the upcrossing rate response \hat{r}_{uc} will be a linear function of the modulated moments (see Appendix A).

The strategy is similar to that taken for the steady state but with Eqs. (6)–(10) solved in the frequency domain. The calculation is algebraically lengthy so here we provide the high-frequency asymptotics with the full forms given in the Appendix. At the mean level

$$\langle \hat{V} \rangle \sim \frac{\bar{\mathcal{E}}_e \hat{\alpha}_e}{(i\omega)^2 \tau_e} \quad \text{and} \quad \langle \hat{V} \rangle \sim \frac{\bar{\mathcal{E}}_e \hat{\alpha}_e}{i\omega \tau_e}, \quad (14)$$

so the rate-of-change of the average voltage is the dominant deterministic contribution to the upcrossing-rate response at higher frequencies.

For the fluctuating components, the driving excitatory synaptic modulation is again delta correlated in space $\langle \hat{h}_e^2 \rangle_x = \delta(x) \hat{\alpha}_e \lambda_e / 2\tau_e (1 + i\omega\tau_e/2)$ but with a frequency-dependent amplitude due to synaptic filtering. Using this result, solving for the response of the voltage and synaptic covariances, the high-frequency asymptote of the voltage variance is found:

$$\langle \hat{v}^2 \rangle \sim -\frac{2\hat{\alpha}_e \tau_v \langle \hat{v}^2 \rangle}{i\omega \tau_e i\omega \tau_v} \quad (15)$$

and so decays as $1/\omega^2$. From $\langle \hat{v}\hat{v} \rangle = (i\omega/2)\langle \hat{v}^2 \rangle$ this also gives the weaker decay of $\langle \hat{v}\hat{v} \rangle \sim 1/i\omega$. Finally, the asymptote of the variance of the rate-of-change of voltage

$$\langle \hat{\dot{v}}^2 \rangle \sim \hat{\alpha}_e \tau_v \frac{\bar{\mathcal{E}}_e^2 \lambda_e}{2\tau_e^2 \lambda_v} \frac{1}{\sqrt{2i\omega\tau_v}} \quad (16)$$

can be seen to have the weakest decay and therefore is dominant at high frequencies.

This is the key and somewhat surprising result for the dynamics of the dendritic model: the high-frequency asymptotics decay as $1/\sqrt{i\omega}$ and, through its linear dependence on $\langle \hat{\dot{v}}^2 \rangle$ as seen in Eq. (A9) of Appendix A, so also must the high-frequency response of the firing rate in the upcrossing approximation

$$\frac{\hat{r}_{uc}}{\bar{r}_{uc}} \sim \hat{\alpha}_e \tau_v \frac{\bar{\mathcal{E}}_e^2 \lambda_e}{4\tau_e^2 \langle \hat{\dot{v}}^2 \rangle \lambda_v} \frac{1}{\sqrt{2i\omega\tau_v}}. \quad (17)$$

This can be contrasted to the result for the isopotential point-neuron model that has an upcrossing response decaying as $1/i\omega$ at higher frequencies (see Ref. [15] and Appendix C). In Figs. 3(d) and 3(e), an illustration of the amplitude and phase of the response is shown. These frequency-domain results are compatible with the earlier observation in Fig. 1(b) that EPSPs on a dendrite can be sharper in time than for an isopotential model.

V. DISCUSSION

The analyses presented here are predicated on a number of biophysical approximations and therefore should be considered as providing the basis for future refinement.

First, the membrane model does not include voltage-gated currents such as the h-current that can affect low frequency components of the firing-rate response. These could be included using a quasioactive membrane approximation [21,22] with additional state variables coupled to the voltage dynamics.

The minimal model presented here also approximates spatial extent as infinite (valid for dendrites significantly longer than the effective electrotonic length λ_v), is homogeneous and has no increased conductance at the position $x = 0$ of the nominal soma. Recent analysis [9] showed significant effects of geometry on the functional forms of steady-state upcrossing rates. The derivation of Eqs. (6)–(10) rely on a long, homogeneous approximation and so adaptation of the method to more realistic geometries might be a technical challenge, though the spatial-mode expansion technique used by Tuckwell [6] is a potential strategy to account for closed-end effects.

A number of approximations of the synaptic drive have been made including the Gaussian approximation of finite-amplitude shot noise. This typically has validity when statistically independent, high-rate, low-amplitude inputs are summed. Given the distinct response seen in isopotential neurons when shot noise is included [23,24], a worthwhile extension would be to examine finite-amplitude effects on the dynamics. This is particularly important for spatiotemporal integration as the relative number of summed inputs within an effective electrotonic length will be less than the global input into an isopotential model.

Finally, though widely used in neuroscience, the upcrossing approximation should be critically evaluated in this spatial context and compared to biophysical models of spike generation. Rapid responses have already been identified in these models due to spiking nonlinearities or somatic-dendritic coupling [25–30]. Extensions of the current study could examine the high-frequency response when both stochastic spatiotemporal integration and nonlinearities known to affect the rapidity of action-potential generation are combined.

ACKNOWLEDGMENTS

We would like to thank Nicolas Brunel and Benjamin Lindner for their useful comments on an earlier version of this manuscript. We also acknowledge funding from the Engineering and Physical Sciences Research Council funding under Grant No. EP/L015374/1 to R.P.G.

APPENDIX A: UPCROSSING-RATE DYNAMICS

The time-dependent rate $r_{uc}(t)$ that a fluctuating membrane voltage V crosses a threshold V_{th} from below is considered. Following Rice [10], this can be written as

$$r_{uc}(t) = \int_0^\infty d\dot{V} \dot{V} \Psi(V_{th}, \dot{V}), \quad (A1)$$

where \dot{V} is the rate-of-change of voltage and $\Psi(V, \dot{V})$ is the joint probability density. The derivations that will be used for the dynamics, steady state and linear response were given by Badel [15] in the context of a related isopotential neuronal model. We repeat that derivation and provide intermediate steps for transparency.

It is first convenient to expand the voltage and its rate of change around their time-dependent mean values $\langle V \rangle$ and $\langle \dot{V} \rangle$ so the fluctuating excesses v and \dot{v} have zero mean: for example, $V(t) = \langle V \rangle + v$. Writing the joint distribution for v and \dot{v} as the conditional distribution $\psi(\dot{v}|v)$ multiplied by the marginal voltage density $\phi(v)$ we have

$$r_{\text{uc}}(t) = \phi(v_{\text{th}}) \int_{-\langle \dot{V} \rangle}^{\infty} d\dot{v} (\langle \dot{V} \rangle + \dot{v}) \psi(\dot{v}|v_{\text{th}}), \quad (\text{A2})$$

where $v_{\text{th}}(t) = V_{\text{th}} - \langle V \rangle$. For the Gaussian-distributed voltages considered in this paper, the distributions can be written as

$$\phi(v) = \frac{1}{\sqrt{2\pi\langle v^2 \rangle}} \exp\left(-\frac{v^2}{2\langle v^2 \rangle}\right), \quad \text{and} \quad (\text{A3})$$

$$\psi(\dot{v}|v) = \frac{1}{\sqrt{2\pi s^2}} \exp\left(-\frac{(\dot{v} - \kappa v)^2}{2s^2}\right), \quad (\text{A4})$$

where the variances $\langle v^2 \rangle$, $\langle \dot{v}^2 \rangle$, covariance $\langle v\dot{v} \rangle$, and other parameters $\kappa = \langle v\dot{v} \rangle / \langle v^2 \rangle$ and $s^2 = \langle \dot{v}^2 \rangle - \kappa^2 \langle v^2 \rangle$ are all potentially time dependent. Using these results for the upcrossing rate we get

$$r_{\text{uc}}(t) = \frac{1}{2\pi} \sqrt{\frac{s^2}{\langle v^2 \rangle}} e^{-v_{\text{th}}^2/2\langle v^2 \rangle} \int_{-\beta}^{\infty} du (2u + 2\beta) e^{-u^2}, \quad (\text{A5})$$

where $\beta = (\langle \dot{V} \rangle + \kappa v_{\text{th}}) / \sqrt{2s^2}$. The integral can be rewritten in terms of Gaussians and the error function

$$r_{\text{uc}}(t) = \frac{1}{2\pi} \sqrt{\frac{s^2}{\langle v^2 \rangle}} e^{-v_{\text{th}}^2/2\langle v^2 \rangle} (e^{-\beta^2} + \sqrt{\pi} \beta [1 + \text{erf}(\beta)]), \quad (\text{A6})$$

which is identical to the result arrived at by Badel [15]. An example of the upcrossing rate in a regime that is nonlinear in the synaptic driving terms is illustrated in Fig. 2(c) (lower panel).

1. Steady-state upcrossing rate

For a quantity $Q(t)$ evaluated in the steady state we use the notation \bar{Q} . The steady-state upcrossing rate simplifies because $\langle \bar{V} \rangle = 0$ and $\langle \bar{v}\bar{\dot{v}} \rangle = \partial_i \langle \bar{v}^2 \rangle / 2 = 0$ so that $\bar{\beta} = 0$ and $\bar{s}^2 = \langle \bar{\dot{v}}^2 \rangle$, giving

$$\bar{r}_{\text{uc}} = \frac{1}{2\pi} \sqrt{\frac{\langle \bar{\dot{v}}^2 \rangle}{\langle \bar{v}^2 \rangle}} \exp\left(-\frac{\bar{v}_{\text{th}}^2}{2\langle \bar{v}^2 \rangle}\right), \quad (\text{A7})$$

where $\bar{v}_{\text{th}} = V_{\text{th}} - \langle \bar{V} \rangle$. Figure 3(c) provides an illustration of the steady-state upcrossing rate.

2. Linear response of the upcrossing rate

We now consider a weak harmonic modulation of the incoming presynaptic rates. This will induce weak modulations, with some amplitude and phase shift, in any dependent

quantity $Q(t)$ that we can conveniently write in complex form $Q(t) = \bar{Q} + \hat{Q}e^{i\omega t}$. Before expanding the upcrossing form, let us examine some of the component quantities. For β and s^2 we have

$$\hat{\beta} = \frac{1}{\sqrt{2\langle \bar{\dot{v}}^2 \rangle}} \left(\langle \hat{V} \rangle + \bar{v}_{\text{th}} \frac{\langle \hat{v}\hat{\dot{v}} \rangle}{\langle \bar{v}^2 \rangle} \right) \quad \text{and} \quad \hat{s}^2 = \langle \hat{\dot{v}}^2 \rangle. \quad (\text{A8})$$

Then, for the upcrossing rate itself, we get that the ratio of the modulation to the steady-state rate is [15]

$$\frac{\hat{r}_{\text{uc}}}{\bar{r}_{\text{uc}}} = \frac{\bar{v}_{\text{th}}}{\langle \bar{v}^2 \rangle} \langle \hat{V} \rangle + \sqrt{\frac{\pi}{2\langle \bar{\dot{v}}^2 \rangle}} \langle \hat{V} \rangle + \frac{1}{2} \frac{\langle \hat{v}^2 \rangle}{\langle \bar{v}^2 \rangle} \left(\frac{\bar{v}_{\text{th}}^2}{\langle \bar{v}^2 \rangle} - 1 \right) + \sqrt{\frac{\pi}{2\langle \bar{v}^2 \rangle}} \bar{v}_{\text{th}} \frac{\langle \hat{v}\hat{\dot{v}} \rangle}{\langle \bar{v}^2 \rangle} + \frac{1}{2} \frac{\langle \hat{\dot{v}}^2 \rangle}{\langle \bar{\dot{v}}^2 \rangle}. \quad (\text{A9})$$

In the above equation, the first two terms provide the deterministic contribution and the last three terms are contributions from modulated fluctuating quantities. The amplitude and phase of the upcrossing linear response is shown in Figs. 3(d) and 3(e), respectively.

APPENDIX B: DENDRITIC MODEL

The differential equations for the deterministic (mean) components in Eq. (3) and the partial differential equations for the fluctuating components (covariances) in Eqs. (6)–(10) completely determine the moment dynamics in the Gaussian approximation of the model. These equations are driven by the ratelike terms $\alpha_e(t)$, $\alpha_i(t)$ that are proportional to the presynaptic excitatory and inhibitory rates. Also appearing in the equations are the total conductance $\mathcal{H}(t) = \alpha_e + (H_e) + (H_i)$ and electromotive forcing terms $\mathcal{E}_s(t) = E_s - \langle V \rangle$. Together, these equations represent a feedforward cascade that provide all the required quantities needed for the upcrossing rate.

There are a number of approaches that can be taken to find the solution of these equations in the steady state or at the linear-response level; for example, direct solution in space using substitution for the inhomogeneous components or using spatial Fourier transforms. Here we will use the former real-space approach and therefore, the following result will often be useful

$$\partial_x^2 \psi = k^2 \psi - 2k\delta(x)\psi_0$$

$$\text{with solution } \psi = \psi_0 e^{-|x|k}. \quad (\text{B1})$$

1. Steady state: dendritic model

We first derive the various same-time space-separated covariances in the steady state as these will be used to calculate the time dependence.

Synaptic autocovariances $\langle \bar{h}_s^2 \rangle_x$. From Eq. (6), these are simply delta correlated in space

$$\langle \bar{h}_s^2 \rangle_x = \delta(x) \frac{\bar{\alpha}_s \lambda_s}{2\tau_s}. \quad (\text{B2})$$

Voltage and synaptic covariances $\langle \overline{vh_s} \rangle_x$. In the steady-state, Eq. (7) reduces to

$$D \frac{\partial^2}{\partial x^2} \langle \overline{vh_s} \rangle_x = \left(\frac{1}{\tau_s} + \frac{1}{\tau_v} \right) \langle \overline{vh_s} \rangle_x - \overline{\mathcal{E}}_s \langle \overline{h_s^2} \rangle_x. \quad (\text{B3})$$

Remembering that $D = \lambda_v^2 / \tau_v$ and looking at the form of Eq. (B1) identifies $\lambda_v^2 k_s^2 = (\tau_v + \tau_s) / \tau_s$. From the prefactor of the delta correlated inhomogeneous term, the solution must therefore be

$$\begin{aligned} \langle \overline{vh_s} \rangle_x &= \frac{1}{2\lambda_v k_s} \left[\frac{\overline{\mathcal{E}}_s}{2\tau_s} \alpha_s \tau_v \frac{\lambda_s}{\lambda_v} \right] e^{-|x|k_s} \\ &= \frac{\overline{\mathcal{E}}_s}{4\tau_s} \alpha_s \tau_v \frac{\lambda_s}{\lambda_v} \sqrt{\frac{\tau_s}{\tau_s + \tau_v}} e^{-|x|k_s}. \end{aligned} \quad (\text{B4})$$

Voltage autocovariance $\langle \overline{v^2} \rangle_x$. There are two inhomogeneous terms in its equation

$$D \frac{\partial^2}{\partial x^2} \langle \overline{v^2} \rangle_x = \frac{1}{\tau_v} \langle \overline{v^2} \rangle_x - \overline{\mathcal{E}}_e \langle \overline{vh_e} \rangle_x - \overline{\mathcal{E}}_i \langle \overline{vh_i} \rangle_x \quad (\text{B5})$$

so it can be resolved into $\langle \overline{v^2} \rangle_x = \langle \overline{v^2} \rangle_x^e + \langle \overline{v^2} \rangle_x^i$. Trying $\langle \overline{v^2} \rangle_x^s = \psi_s + c_s \langle \overline{vh_s} \rangle_x$ and using Eq. (B3) to remove the double derivative requires setting $c_s = -\tau_s \overline{\mathcal{E}}_s$ to cancel the inhomogeneous term. This leaves

$$D \frac{\partial^2}{\partial x^2} \psi_s = \frac{1}{\tau_v} \psi_s - \overline{\mathcal{E}}_s^2 \tau_s \langle \overline{h_s^2} \rangle_x. \quad (\text{B6})$$

Introducing $k_v^2 = 1/\lambda_v^2$, the solution for ψ_s is

$$\psi_s = \frac{\overline{\mathcal{E}}_s^2}{4} \alpha_s \tau_v \frac{\lambda_e}{\lambda_v} e^{-|x|k_v}. \quad (\text{B7})$$

Putting these forms in $\langle \overline{v^2} \rangle_x^s = \psi_s + c_s \langle \overline{vh_s} \rangle_x$ gives

$$\langle \overline{v^2} \rangle_x^s = \left(\frac{\overline{\mathcal{E}}_s^2}{4} \alpha_s \tau_v \frac{\lambda_s}{\lambda_v} \right) \left(e^{-|x|k_v} - \sqrt{\frac{\tau_s}{\tau_v + \tau_s}} e^{-|x|k_s} \right). \quad (\text{B8})$$

It can be noted that this gives the voltage autocovariance a zero gradient at $x = 0$.

Rate-of-change-of-voltage autocovariance $\langle \overline{\dot{v}^2} \rangle_x$. In the steady-state this is simply

$$\langle \overline{\dot{v}^2} \rangle_x = \frac{\overline{\mathcal{E}}_e}{\tau_e} \langle \overline{vh_e} \rangle_x + \frac{\overline{\mathcal{E}}_i}{\tau_i} \langle \overline{vh_i} \rangle_x, \quad (\text{B9})$$

where the forms for $\langle \overline{vh_s} \rangle_x$ have already been given above.

2. Deterministic weak oscillations: dendritic model

Modulation of the excitatory presynaptic drive $\hat{\alpha}_e$ only is considered, so the modulated inhibitory drive is zero $\hat{\alpha}_i = 0$. With this in mind, expanding the deterministic equations [Eq. (3)] at the level of the linear response to excitatory oscillations gives the following quantities of interest

$$\langle \widehat{H}_e \rangle = \widehat{\mathcal{H}} = \frac{\hat{\alpha}_e}{1 + i\omega\tau_e} \quad \text{and} \quad \langle \widehat{H}_i \rangle = 0, \quad (\text{B10})$$

so

$$\langle \widehat{V} \rangle = \frac{\overline{\mathcal{E}}_s \langle \widehat{H}_e \rangle}{1/\tau_v + i\omega} = \frac{\hat{\alpha}_e \tau_v \overline{\mathcal{E}}_s}{(1 + i\omega\tau_s)(1 + i\omega\tau_v)}, \quad (\text{B11})$$

and the modulated rate-of-change of the voltage is given by $\langle \widehat{\dot{V}} \rangle = i\omega \langle \widehat{V} \rangle$. Note also that $\widehat{\mathcal{E}}_s = -\langle \widehat{V} \rangle$ for $s = e, i$.

3. Weak oscillations and fluctuations: dendritic model

We present the modulated moment derivations in the order of the cascade of equations, remembering again that for modulated excitatory drive only we have $\hat{\alpha}_i = 0$ throughout.

Synaptic autocovariances $\langle \widehat{h_s^2} \rangle_x$. These are delta correlated

$$\langle \widehat{h_e^2} \rangle_x = \delta(x) \frac{\hat{\alpha}_e \lambda_e}{2\tau_e} \frac{1}{1 + i\omega\tau_e/2} \quad \text{and} \quad \langle \widehat{h_i^2} \rangle_x = 0. \quad (\text{B12})$$

Voltage and synaptic covariances $\langle \widehat{vh_s} \rangle_x$. This obeys

$$\begin{aligned} D \partial_x^2 \langle \widehat{vh_s} \rangle_x &= \left(i\omega + \frac{1}{\tau_v} + \frac{1}{\tau_s} \right) \langle \widehat{vh_s} \rangle_x \\ &+ \widehat{\mathcal{H}} \langle \overline{vh_s} \rangle_x - \overline{\mathcal{E}}_s \langle \widehat{h_s^2} \rangle_x - \widehat{\mathcal{E}}_s \langle \overline{h_s^2} \rangle_x. \end{aligned} \quad (\text{B13})$$

We then use a substitution of the form $\langle \widehat{vh_s} \rangle_x = \psi_s + a_s \langle \overline{vh_s} \rangle_x$ and use the result of Eq. (B3) to remove the double spatial derivative on $\langle \widehat{vh_s} \rangle_x$. Setting $a_s = -\widehat{\mathcal{H}}/i\omega$ then removes the remaining inhomogeneous term in $\langle \widehat{vh_s} \rangle_x$ to leave

$$\partial_x^2 \psi_s = \hat{k}_s^2 \psi_s - \frac{\overline{\mathcal{E}}_s}{D} \langle \widehat{h_s^2} \rangle_x - \frac{1}{D} (\widehat{\mathcal{E}}_s - a_s \overline{\mathcal{E}}_e) \langle \overline{h_s^2} \rangle_x,$$

where $\lambda_v^2 \hat{k}_s^2 = (1 + \tau_v/\tau_s + i\omega\tau_v)$. This is straightforwardly solved and, when combined with the other inhomogeneous term, gives

$$\begin{aligned} \langle \widehat{vh_s} \rangle_x &= \frac{1}{4\tau_s} \frac{\lambda_s}{\lambda_v} \left(\frac{\overline{\mathcal{E}}_s \alpha_s \tau_v}{1 + i\omega\tau_s/2} + \widehat{\mathcal{E}}_s \alpha_s \tau_v + \frac{\widehat{\mathcal{H}} \overline{\mathcal{E}}_s}{i\omega} \alpha_s \tau_v \right) \frac{e^{-|x|k_s}}{\hat{k}_s \lambda_v} \\ &- \frac{\widehat{\mathcal{H}}}{i\omega} \langle \overline{vh_s} \rangle_x. \end{aligned} \quad (\text{B14})$$

Note that we would have $\hat{\alpha}_i = 0$ in the first term for the inhibitory form $\langle \widehat{vh_i} \rangle_x$.

Voltage autocovariance $\langle \widehat{v^2} \rangle_x$. This obeys

$$\begin{aligned} D \partial_x^2 \langle \widehat{v^2} \rangle_x &= \left(\frac{i\omega}{2} + \frac{1}{\tau_v} \right) \langle \widehat{v^2} \rangle_x + \widehat{\mathcal{H}} \langle \overline{v^2} \rangle_x \\ &- \overline{\mathcal{E}}_e \langle \widehat{vh_e} \rangle_x - \widehat{\mathcal{E}}_e \langle \overline{vh_e} \rangle_x - \overline{\mathcal{E}}_i \langle \widehat{vh_i} \rangle_x - \widehat{\mathcal{E}}_i \langle \overline{vh_i} \rangle_x. \end{aligned} \quad (\text{B15})$$

We can separate this into components for excitation and inhibition, each of which satisfies

$$\begin{aligned} D \partial_x^2 \langle \widehat{v^2} \rangle_x^s &= \left(\frac{i\omega}{2} + \frac{1}{\tau_v} \right) \langle \widehat{v^2} \rangle_x^s + \widehat{\mathcal{H}} \langle \overline{v^2} \rangle_x^s \\ &- \overline{\mathcal{E}}_s \langle \widehat{vh_s} \rangle_x - \widehat{\mathcal{E}}_s \langle \overline{vh_s} \rangle_x. \end{aligned} \quad (\text{B16})$$

These can be solved by substituting $\langle \widehat{v^2} \rangle_x^s = a \langle \overline{v^2} \rangle_x^s + b_s \langle \widehat{vh_s} \rangle_x + c_s \langle \overline{vh_s} \rangle_x + \psi_s$, giving

$$\begin{aligned} a D \partial_x^2 \langle \overline{v^2} \rangle_x^s &+ b_s D \partial_x^2 \langle \widehat{vh_s} \rangle_x + c_s D \partial_x^2 \langle \overline{vh_s} \rangle_x + D \partial_x^2 \psi_s \\ &= \left(\frac{i\omega}{2} + \frac{1}{\tau_v} \right) (a \langle \overline{v^2} \rangle_x^s + b_s \langle \widehat{vh_s} \rangle_x + c_s \langle \overline{vh_s} \rangle_x + \psi_s) \\ &+ \widehat{\mathcal{H}} \langle \overline{v^2} \rangle_x^s - [\overline{\mathcal{E}}_s \langle \widehat{vh_s} \rangle_x + \widehat{\mathcal{E}}_s \langle \overline{vh_s} \rangle_x]. \end{aligned} \quad (\text{B17})$$

We now replace the double spatial derivatives $D\partial_x^2\langle\widehat{v^2}\rangle_x^s$, $D\partial_x^2\langle\widehat{vh_s}\rangle_x$, and $D\partial_x^2\langle\widehat{v\overline{h_s}}\rangle_x$ using Eq. (B5) resolved into s-dependent components for $\langle\widehat{v^2}\rangle_x^s$ as well as Eqs. (B13) and (B3), respectively, for $\langle\widehat{vh_s}\rangle_x$ and $\langle\widehat{v\overline{h_s}}\rangle_x$, to give

$$\begin{aligned} & a\left[\frac{1}{\tau_v}\langle\widehat{v^2}\rangle_x^s - \overline{\mathcal{E}_s}\langle\widehat{v\overline{h_s}}\rangle_x\right] + b_s\left[\left(i\omega + \frac{1}{\tau_v} + \frac{1}{\tau_s}\right)\langle\widehat{vh_s}\rangle_x\right. \\ & \quad \left. + \widehat{\mathcal{H}}\langle\widehat{v\overline{h_s}}\rangle_x - \overline{\mathcal{E}_s}\langle\widehat{h_s^2}\rangle_x - \widehat{\mathcal{E}_s}\langle\widehat{\overline{h_s^2}}\rangle_x\right] \\ & + c_s\left[\left(\frac{1}{\tau_v} + \frac{1}{\tau_s}\right)\langle\widehat{v\overline{h_s}}\rangle_x - \overline{\mathcal{E}_s}\langle\widehat{\overline{h_s^2}}\rangle_x\right] + D\partial_x^2\psi \\ & = \left(\frac{i\omega}{2} + \frac{1}{\tau_v}\right)\left(a\langle\widehat{v^2}\rangle_x^s + b_s\langle\widehat{vh_s}\rangle_x + c_s\langle\widehat{v\overline{h_s}}\rangle_x + \psi_s\right) \\ & + \widehat{\mathcal{H}}\langle\widehat{v^2}\rangle_x^s - \overline{\mathcal{E}_s}\langle\widehat{v\overline{h_s}}\rangle_x - \widehat{\mathcal{E}_s}\langle\widehat{v\overline{h_s}}\rangle_x. \end{aligned} \tag{B18}$$

We then set a , b_s , and c_s to remove the inhomogeneous terms in $\langle\widehat{v^2}\rangle_x^s$, $\langle\widehat{vh_s}\rangle_x$, and $\langle\widehat{v\overline{h_s}}\rangle_x$, respectively:

$$\begin{aligned} a &= -\frac{2\widehat{\mathcal{H}}}{i\omega}, \quad b_s = \frac{-\overline{\mathcal{E}_s}\tau_s}{1 + i\omega\tau_s/2}, \\ \text{and } c_s &= \frac{\tau_s(a\overline{\mathcal{E}_s} - \widehat{\mathcal{E}_s} - b_s\widehat{\mathcal{H}})}{1 - i\omega\tau_s/2} \end{aligned} \tag{B19}$$

and leave an equation for ψ_s of the form

$$\begin{aligned} D\partial_x^2\psi_s &= \left(\frac{i\omega}{2} + \frac{1}{\tau_v}\right)\psi_s \\ & + b_s\overline{\mathcal{E}_s}\langle\widehat{h_s^2}\rangle_x + b_s\widehat{\mathcal{E}_s}\langle\widehat{\overline{h_s^2}}\rangle_x + c_s\overline{\mathcal{E}_s}\langle\widehat{\overline{h_s^2}}\rangle_x. \end{aligned} \tag{B20}$$

This equation has solution

$$\begin{aligned} \psi_s &= -\frac{1}{4\tau_s}\frac{\lambda_s}{\lambda_v}\left[b_s\left(\frac{\overline{\mathcal{E}_s}\hat{\alpha}_s\tau_v}{1 + i\omega\tau_s/2} + \widehat{\mathcal{E}_s}\hat{\alpha}_s\tau_v\right) + c_s\overline{\mathcal{E}_s}\hat{\alpha}_s\tau_v\right] \\ & \times \frac{e^{-|x|\hat{k}_v}}{\lambda_v\hat{k}_v} \end{aligned} \tag{B21}$$

which, together with the other inhomogeneous forms in $\langle\widehat{v^2}\rangle_x^s = a\langle\widehat{v^2}\rangle_x^s + b_s\langle\widehat{vh_s}\rangle_x + c_s\langle\widehat{v\overline{h_s}}\rangle_x + \psi_s$ completes the solution for one synaptic component of the modulated variance.

Rate-of-change of voltage autocovariance $\langle\widehat{v\dot{v}}\rangle_x$. This has form

$$\begin{aligned} \langle\widehat{v\dot{v}}\rangle_x &= \overline{\mathcal{E}_e}\langle\widehat{v\dot{h}_e}\rangle_x + \widehat{\mathcal{E}_e}\langle\widehat{v\dot{h}_e}\rangle_x + \overline{\mathcal{E}_i}\langle\widehat{v\dot{h}_i}\rangle_x + \widehat{\mathcal{E}_i}\langle\widehat{v\dot{h}_i}\rangle_x \\ & - \frac{1}{\tau_v}\langle\widehat{v\dot{v}}\rangle_x + D\partial_x^2\langle\widehat{v\dot{v}}\rangle_x. \end{aligned} \tag{B22}$$

We again separate out the solution in terms of the components involving excitation and inhibition

$$\begin{aligned} \langle\widehat{v^2}\rangle_x^s &= \frac{\overline{\mathcal{E}_s}}{\tau_s}(1 + i\omega\tau_s)\langle\widehat{vh_s}\rangle_x + \frac{\widehat{\mathcal{E}_s}}{\tau_s}\langle\widehat{v\overline{h_s}}\rangle_x \\ & - \frac{i\omega}{2\tau_v}\langle\widehat{v^2}\rangle_x^s + \frac{i\omega}{2}D\partial_x^2\langle\widehat{v^2}\rangle_x^s, \end{aligned} \tag{B23}$$

where we have also made use of the simplifying relations for $\langle\widehat{vh_s}\rangle_x$ and $\langle\widehat{v\dot{v}}\rangle_x$ in the steady-state and linear-response levels.

We now substitute for the following term

$$\begin{aligned} D\partial_x^2\langle\widehat{v^2}\rangle_x^s &= \left(\frac{i\omega}{2} + \frac{1}{\tau_v}\right)\langle\widehat{v^2}\rangle_x^s \\ & + \widehat{\mathcal{H}}\langle\widehat{v^2}\rangle_x^s - \overline{\mathcal{E}_s}\langle\widehat{v\overline{h_s}}\rangle_x - \widehat{\mathcal{E}_s}\langle\widehat{v\overline{h_s}}\rangle_x \end{aligned} \tag{B24}$$

and tidy things up to get

$$\begin{aligned} \langle\widehat{v^2}\rangle_x^s &= \frac{\overline{\mathcal{E}_s}}{\tau_s}\left(1 + \frac{i\omega\tau_s}{2}\right)\langle\widehat{vh_s}\rangle_x + \frac{\widehat{\mathcal{E}_s}}{\tau_s}\left(1 - \frac{i\omega\tau_s}{2}\right)\langle\widehat{v\overline{h_s}}\rangle_x \\ & + \left(\frac{i\omega}{2}\right)^2\langle\widehat{v^2}\rangle_x^s + \frac{i\omega}{2}\widehat{\mathcal{H}}\langle\widehat{v^2}\rangle_x^s \end{aligned} \tag{B25}$$

which is expressed in terms of quantities already derived.

4. Low-frequency limit: dendritic model

In the limit $\omega \rightarrow 0$, the various frequency-dependent quantities $\widehat{Q}(\omega)$ can be obtained by taking derivatives of corresponding steady-state quantities with respect to $\hat{\alpha}_e$,

$$\lim_{\omega \rightarrow 0}\widehat{Q} = \hat{\alpha}_e\frac{d}{d\hat{\alpha}_e}\overline{Q}, \tag{B26}$$

where it should be remembered that τ_v , λ_v , $\overline{\mathcal{E}_e}$, $\overline{\mathcal{E}_i}$ all depend on $\hat{\alpha}_e$. The following results are useful

$$\begin{aligned} \frac{d}{d\hat{\alpha}_e}\frac{1}{\tau_v} &= 1, \quad \frac{d}{d\hat{\alpha}_e}\tau_v = -\tau_v^2, \\ \frac{d}{d\hat{\alpha}_e}\overline{\mathcal{E}_s} &= -\frac{d}{d\hat{\alpha}_e}\langle\overline{V}\rangle = -\tau_v\overline{\mathcal{E}_e}, \quad \text{and } \frac{d}{d\hat{\alpha}_e}\frac{1}{\lambda_v} = \frac{1}{2}\frac{\tau_v}{\lambda_v}. \end{aligned} \tag{B27}$$

It is also useful to introduce the following definition and its derivatives:

$$x_s = \frac{\tau_s}{\tau_s + \tau_v} \text{ so } \frac{d}{d\hat{\alpha}_e}x_s = \tau_v x_s(1 - x_s) = \frac{\tau_v^2}{\tau_s}x_s^2. \tag{B28}$$

Finally, note that because \dot{V} or $\langle\widehat{v\dot{v}}\rangle_x$ are both complete temporal derivatives, their temporal Fourier transforms vanish in the $\omega = 0$. We now provide the forms of the remaining moments.

Voltage and synaptic covariance $\langle\widehat{vh_s}\rangle_x$. In terms of x_e and x_i , these can be written

$$\begin{aligned} \lim_{\omega \rightarrow 0}\langle\widehat{vh_e}\rangle_x &= \hat{\alpha}_e\tau_v\frac{\overline{\mathcal{E}_e}}{4\tau_e}\frac{\lambda_e}{\lambda_v}\sqrt{x_e}\left(1 - \hat{\alpha}_e\tau_v\left(1 + \frac{x_e}{2}\right)\right), \\ \lim_{\omega \rightarrow 0}\langle\widehat{vh_i}\rangle_x &= -\hat{\alpha}_e\tau_v\frac{1}{4\tau_i}\frac{\lambda_i}{\lambda_v}\sqrt{x_i}\hat{\alpha}_i\tau_v\left(\overline{\mathcal{E}_e} + \overline{\mathcal{E}_i}\frac{x_i}{2}\right). \end{aligned} \tag{B29}$$

Voltage variance $\langle\widehat{v^2}\rangle_x$. We can split this term into excitatory and inhibitory components and use the same definitions for x_e and x_i as above

$$\begin{aligned} \lim_{\omega \rightarrow 0}\langle\widehat{v^2}\rangle_x^e &= \hat{\alpha}_e\tau_v\frac{\overline{\mathcal{E}_e}^2}{4}\frac{\lambda_e}{\lambda_v}\left(\left(1 - 2\hat{\alpha}_e\tau_v\right)\left(1 - \sqrt{x_e}\right)\right. \\ & \quad \left. - \frac{\hat{\alpha}_e\tau_v}{2}\left(1 - \sqrt{x_e^3}\right)\right), \\ \lim_{\omega \rightarrow 0}\langle\widehat{v^2}\rangle_x^i &= -\hat{\alpha}_e\tau_v\frac{1}{4}\frac{\lambda_i}{\lambda_v}\hat{\alpha}_i\tau_v\left(2\overline{\mathcal{E}_e}\overline{\mathcal{E}_i}\left(1 - \sqrt{x_i}\right)\right. \\ & \quad \left. + \frac{\overline{\mathcal{E}_i}^2}{2}\left(1 - \sqrt{x_i^3}\right)\right). \end{aligned} \tag{B30}$$

Rate-of-change of voltage variance $\langle \widehat{v}^2 \rangle$. The excitatory and inhibitory components are proportional to $\langle \widehat{vh}_e \rangle$ and $\langle \widehat{vh}_i \rangle$ so that

$$\begin{aligned} \lim_{\omega \rightarrow 0} \langle \widehat{v}^2 \rangle^e &= \hat{\alpha}_e \tau_v \frac{\bar{\mathcal{E}}_e^2 \lambda_e}{4\tau_e^2 \lambda_v} \sqrt{x_e} \left(1 - \bar{\alpha}_e \tau_v \left(2 + \frac{x_e}{2} \right) \right), \\ \lim_{\omega \rightarrow 0} \langle \widehat{v}^2 \rangle^i &= -\hat{\alpha}_e \tau_v \frac{1}{4\tau_e^2} \frac{\lambda_i}{\lambda_v} \sqrt{x_i} \bar{\alpha}_i \tau_v \left(2\bar{\mathcal{E}}_e \bar{\mathcal{E}}_i + \bar{\mathcal{E}}_i^2 \frac{x_i}{2} \right). \end{aligned} \quad (\text{B31})$$

5. High-frequency asymptotics: dendritic model

For a modulation of the excitatory component, to leading order, the deterministic components needed are

$$\begin{aligned} \langle \widehat{V} \rangle &\sim \frac{\hat{\alpha}_e \bar{\mathcal{E}}_e}{(i\omega)^2 \tau_e}, \quad \langle \widehat{V} \rangle \sim \frac{\hat{\alpha}_e \bar{\mathcal{E}}_e}{i\omega \tau_e}, \\ \langle \widehat{H}_e \rangle &= \widehat{\mathcal{H}} \sim \frac{\hat{\alpha}_e}{i\omega \tau_e}, \quad \text{and} \quad \widehat{\mathcal{E}}_e = \widehat{\mathcal{E}}_i = -\langle \widehat{V} \rangle. \end{aligned} \quad (\text{B32})$$

Note that $\langle \widehat{H}_i \rangle = 0$ because $\hat{\alpha}_i = 0$. The dominant contribution to the deterministic component to the upcrossing rate is therefore $1/\omega$ and comes from the rate-of-change of voltage term. We now take the covariances in turn.

Voltage and synaptic covariance $\langle \widehat{vh}_s \rangle$. For the covariances between voltage and synaptic drive we have

$$\begin{aligned} \langle \widehat{vh}_e \rangle &\sim \hat{\alpha}_e \tau_v \frac{\bar{\mathcal{E}}_e \lambda_e}{2\tau_e \lambda_v} \frac{1}{i\omega \tau_e} \frac{1}{\sqrt{i\omega \tau_v}} \quad \text{and} \\ \langle \widehat{vh}_i \rangle &\sim -\frac{\hat{\alpha}_e \tau_v \langle \widehat{vh}_i \rangle}{i\omega \tau_e i\omega \tau_v}. \end{aligned} \quad (\text{B33})$$

Voltage variance $\langle \widehat{v}^2 \rangle$ and $\langle \widehat{vv} \rangle$. Examining the forms of the various terms in Eq. (B19) we see that $a \sim 1/\omega^2$, $b_s \sim 1/\omega$, and $c_s \sim 1/\omega^3$. The term multiplying the exponential therefore decays as $1/\omega^{5/2}$ and is less significant than the $a \langle \widehat{v}^2 \rangle_x^s$ term, which dominates the inhomogeneous parts of the solution. Using the asymptotics for a then gives

$$\langle \widehat{v}^2 \rangle \sim -\frac{\hat{\alpha}_e \tau_v}{i\omega \tau_e} \frac{2}{i\omega \tau_e} \langle \widehat{v}^2 \rangle \quad \text{and} \quad \langle \widehat{vv} \rangle \sim -\frac{\hat{\alpha}_e}{i\omega \tau_e} \langle \widehat{v}^2 \rangle, \quad (\text{B34})$$

where the latter result follows from $\langle \widehat{vv} \rangle = (i\omega/2) \langle \widehat{v}^2 \rangle$.

Rate-of-change of voltage variance $\langle \widehat{v}^2 \rangle$. It is useful to rearrange the form of this equation so that

$$\begin{aligned} \langle \widehat{v}^2 \rangle_x^s &= \left(\frac{i\omega}{2} \right)^2 \left[\langle \widehat{v}^2 \rangle_x^s + \frac{2}{i\omega} \widehat{\mathcal{H}} \langle \widehat{v}^2 \rangle_x^s + \frac{2\bar{\mathcal{E}}_s}{i\omega} \langle \widehat{vh}_s \rangle_x \right] \\ &\quad + \frac{\bar{\mathcal{E}}_s}{\tau_s} \langle \widehat{vh}_s \rangle_x + \frac{\widehat{\mathcal{E}}_s}{\tau_s} \left(1 - \frac{i\omega \tau_s}{2} \right) \langle \widehat{vh}_s \rangle_x. \end{aligned} \quad (\text{B35})$$

To leading order, the part in the square brackets is equivalent to ψ_s in the solution for $\langle \widehat{v}^2 \rangle_x^s$ [see Eq. (B21) and above]. The leading order component of $\psi_s(x=0)$ is

$$\psi_s \sim -\frac{\bar{\mathcal{E}}_s^2 \lambda_s}{4\tau_s^2 \lambda_v} \frac{1}{i\omega/2} \frac{\hat{\alpha}_s \tau_v}{i\omega/2} \frac{1}{\lambda_v \hat{k}_v} \quad (\text{B36})$$

so that we have

$$\langle \widehat{v}^2 \rangle \sim \hat{\alpha}_e \tau_v \frac{\bar{\mathcal{E}}_e^2 \lambda_e}{2\tau_e^2 \lambda_v} \frac{1}{\sqrt{2i\omega \tau_v}}. \quad (\text{B37})$$

APPENDIX C: ISOPOTENTIAL MODEL

As a reference model to compare the additional effect of spatiotemporal filtering we consider an isopotential neuron receiving temporally filtered synaptic drive. This type of model has been analyzed previously [20] including using the upcrossing approximation [15]. The model comprises two synaptic conductances filtered at excitatory and inhibitory time scales τ_e and τ_i . These conductances drive a voltage equation that also includes a leak conductance. As before, it proves convenient to introduce ratelike quantities that are conductances divided by the membrane capacitance.

$$\begin{aligned} \frac{dV}{dt} &= \alpha_\ell (E_\ell - V) + H_e (E_e - V) + H_i (E_i - V), \\ \tau_e \frac{dH_e}{dt} &= \alpha_e - H_e + \sqrt{\alpha_e \kappa_e} \xi_e(t), \\ \tau_i \frac{dH_i}{dt} &= \alpha_i - H_i + \sqrt{\alpha_i \kappa_i} \xi_i(t). \end{aligned} \quad (\text{C1})$$

The time-dependent quantities $\alpha_s(t)$ where $s = e$ or i are proportional to the presynaptic rate whereas the κ_s parameters are constant. We use a Gaussian approximation for the synaptic drive so that $\xi_s(t)$ is a white-noise process with zero mean, autocovariance $\langle \xi_s(t_1) \xi_s(t_2) \rangle = \delta(t_1 - t_2)$ and it is assumed that excitatory and inhibitory synaptic drives are uncorrelated.

Similar to the approach used for the long-dendrite model, we separate voltages and conductances into deterministic and zero-mean fluctuating components $V = \langle V \rangle + v$ and $H_s = \langle H_s \rangle + h_s$. At the level of the stochastic differential equation for voltage, we drop less significant terms that are second order in the fluctuating components like vh_s with the result that v also has Gaussian statistics. In terms of the quantities α_s , the deterministic equations for the isopotential neuron are identical to the dendritic case given in Eq. (3). The fluctuating components, however, obey

$$\begin{aligned} \dot{v} &= h_e \mathcal{E}_e + h_i \mathcal{E}_i - \mathcal{H}v, \\ \tau_e \dot{h}_e &= \sqrt{\alpha_e \kappa_e} \xi_e - h_e, \\ \tau_i \dot{h}_i &= \sqrt{\alpha_i \kappa_i} \xi_i - h_i, \end{aligned} \quad (\text{C2})$$

where we again have the notations $\mathcal{E}_s(t) = E_s - \langle V \rangle$ and $\mathcal{H}(t) = \alpha_\ell + \langle H_e \rangle + \langle H_i \rangle$. Note that the difference between this isopotential reference model and the dendritic case [Eq. (4)] is the absence of a second spatial derivative in the equation for the voltage and that the synaptic quantities are instead driven by temporal Gaussian white noise, not spatiotemporal Gaussian white noise.

1. Voltage-moment equations: isopotential model

The deterministic equation set (3) provides a complete description of dynamics of the first moments $\langle V \rangle$ and $\langle \dot{V} \rangle$. We now derive a set of differential equations for the second moments of the voltage and its derivative. First, we can solve for the variance of one of the synaptic drives. This can be written as filter integral over the quantity $\alpha_s(t)$,

$$\langle h_s^2 \rangle = \frac{\kappa_s}{\tau_s^2} \int_{-\infty}^t dt' \alpha_s(t') e^{-2(t-t')/\tau_s}, \quad (\text{C3})$$

and because the filter is exponential, it can be rewritten in the differential form

$$\frac{\tau_s}{2} \frac{d\langle h_s^2 \rangle}{dt} = \frac{\alpha_s \kappa_e}{2\tau_s} \langle h_s^2 \rangle. \quad (\text{C4})$$

We next crossmultiply the stochastic differential equations for v and h_s by h_s and v , and average to get

$$\langle \dot{v} h_s \rangle = \mathcal{E}_s \langle h_s^2 \rangle - \mathcal{H} \langle v h_s \rangle \text{ and } \langle \dot{v} h_s \rangle = -\langle v h_s \rangle / \tau_s, \quad (\text{C5})$$

where the causality $\langle \xi_s v \rangle = 0$ has been used in the latter equation. Adding these gives the complete derivative $\langle \dot{v} h_s \rangle + \langle v \dot{h}_s \rangle = \partial_t \langle v h_s \rangle$, and so

$$\frac{d\langle v h_s \rangle}{dt} = \mathcal{E}_s \langle h_s^2 \rangle - \left(\mathcal{H} + \frac{1}{\tau_s} \right) \langle v h_s \rangle. \quad (\text{C6})$$

We can also multiply the stochastic differential equation for v by v and average to get

$$\frac{1}{2} \frac{d\langle v^2 \rangle}{dt} = \mathcal{E}_e \langle v h_e \rangle + \mathcal{E}_i \langle v h_i \rangle - \mathcal{H} \langle v^2 \rangle = \langle \dot{v} v \rangle, \quad (\text{C7})$$

which provide equations for both $\langle v^2 \rangle$ and $\langle \dot{v} v \rangle$. For the autocovariance of the rate-of-change of voltage we multiply the differential equation for v by \dot{v} and average

$$\langle \dot{v}^2 \rangle = \mathcal{E}_e \langle \dot{v} h_e \rangle + \mathcal{E}_i \langle \dot{v} h_i \rangle - \mathcal{H} \langle \dot{v} v \rangle. \quad (\text{C8})$$

All together, these differential equations and subsidiary relations for the synaptic drive and voltage provide all that is required to apply the upcrossing method to the isopotential model.

2. Steady state: isopotential model

The steady state $\langle \bar{V} \rangle$ for the mean voltage is identical to that given for the dendritic model; however, the variance and variance of the rate-of-change of voltage are different. First we note that $\langle \bar{h}_s^2 \rangle = \bar{\alpha}_s \kappa_s / 2\tau_s$ and that it is useful to use the steady-state relation $\tau_s \langle \dot{v} h_s \rangle = \langle \bar{v} h_s \rangle$. Then comparing the relevant equations above we have

$$\langle \bar{v}^2 \rangle = \frac{\bar{\mathcal{E}}_e^2}{2} \kappa_e \bar{\alpha}_e \tau_v \frac{\tau_v}{(\tau_v + \tau_e)} + \frac{\bar{\mathcal{E}}_i^2}{2} \kappa_i \bar{\alpha}_i \tau_v \frac{\tau_v}{(\tau_v + \tau_i)} \quad (\text{C9})$$

which can be seen in Fig. 3(b) (middle panel) for a case matched to the dendritic model. For the variance of the rate-of-change of voltage we have

$$\langle \dot{v}^2 \rangle = \frac{\bar{\mathcal{E}}_e^2}{2\tau_e^2} \kappa_e \bar{\alpha}_e \tau_v \frac{\tau_v}{(\tau_v + \tau_e)} + \frac{\bar{\mathcal{E}}_i^2}{2\tau_i^2} \kappa_i \bar{\alpha}_i \tau_v \frac{\tau_v}{(\tau_v + \tau_i)} \quad (\text{C10})$$

which is also illustrated in Fig. 3(b) (lower panel). Other useful quantities are

$$\langle \bar{v} h_e \rangle = \frac{\bar{\mathcal{E}}_e \langle \bar{h}_e^2 \rangle}{\mathcal{H} + 1/\tau_e} \text{ and } \langle \bar{v} h_i \rangle = \frac{\bar{\mathcal{E}}_i \langle \bar{h}_i^2 \rangle}{1 + \tau_e \mathcal{H}}, \quad (\text{C11})$$

and similarly for inhibition.

3. Response to weak oscillations: isopotential model

We again consider a weak oscillation of the excitatory drive such that $\alpha_e(t) = \bar{\alpha}_e + \hat{\alpha}_e e^{i\omega t}$ and keep terms in all calculations up to first order in $\hat{\alpha}_e$. The deterministic, first-order

moments of the various quantities are identical to the case of the long-dendrite considered previously. The second-order moments are different, and for the conductances we have

$$\langle \hat{h}_e^2 \rangle = \frac{\hat{\alpha}_e \kappa_e}{2\tau_e} \frac{1}{1 + i\omega\tau_e/2} \text{ and } \langle \hat{h}_i^2 \rangle = 0. \quad (\text{C12})$$

The next quantities of interest are the covariances between the conductance and voltage

$$\langle \widehat{v} h_e \rangle = \frac{\bar{\mathcal{E}}_e \langle \hat{h}_e^2 \rangle - \langle \widehat{V} \rangle \langle \hat{h}_e^2 \rangle - \widehat{\mathcal{H}} \langle \widehat{v} h_e \rangle}{i\omega + \bar{\mathcal{H}} + 1/\tau_e}, \text{ and}$$

$$\langle \widehat{v} h_i \rangle = -\frac{\langle \widehat{V} \rangle \langle \hat{h}_i^2 \rangle + \widehat{\mathcal{H}} \langle \widehat{v} h_i \rangle}{i\omega + \bar{\mathcal{H}} + 1/\tau_i}, \quad (\text{C13})$$

where $\langle \hat{h}_i^2 \rangle = 0$ has been used. The oscillatory voltage variance can be expressed in terms of these quantities

$$\langle \widehat{v}^2 \rangle = \frac{\bar{\mathcal{E}}_e \langle \widehat{v} h_e \rangle + \bar{\mathcal{E}}_i \langle \widehat{v} h_i \rangle - \langle \widehat{V} \rangle (\langle \widehat{v} h_e \rangle + \langle \widehat{v} h_i \rangle) - \widehat{\mathcal{H}} \langle \widehat{v}^2 \rangle}{i\omega/2 + \bar{\mathcal{H}}}. \quad (\text{C14})$$

The covariance has the relation $\langle \widehat{v} \dot{v} \rangle = i\omega \langle \widehat{v}^2 \rangle / 2$ and is therefore obtained directly from the above. Finally, to calculate the variance of \dot{v} we need

$$\langle \widehat{v} \dot{h}_e \rangle = (\bar{\mathcal{E}}_e \langle \hat{h}_e^2 \rangle - \langle \widehat{V} \rangle \langle \hat{h}_e^2 \rangle - \bar{\mathcal{H}} \langle \widehat{v} h_e \rangle - \widehat{\mathcal{H}} \langle \widehat{v} h_e \rangle),$$

$$\langle \widehat{v} \dot{h}_i \rangle = -(\langle \widehat{V} \rangle \langle \hat{h}_i^2 \rangle + \bar{\mathcal{H}} \langle \widehat{v} h_i \rangle + \widehat{\mathcal{H}} \langle \widehat{v} h_i \rangle), \quad (\text{C15})$$

and the same for inhibition, again noting that $\langle \hat{h}_i^2 \rangle = 0$. We can then write that

$$\langle \widehat{v}^2 \rangle = \bar{\mathcal{E}}_e \langle \widehat{v} \dot{h}_e \rangle + \bar{\mathcal{E}}_i \langle \widehat{v} \dot{h}_i \rangle - \langle \widehat{V} \rangle (\langle \widehat{v} \dot{h}_e \rangle + \langle \widehat{v} \dot{h}_i \rangle) - \bar{\mathcal{H}} \langle \widehat{v} \dot{v} \rangle, \quad (\text{C16})$$

where the steady-state result $\langle \bar{v} \dot{v} \rangle = 0$ has been used.

4. Low-frequency limit: isopotential model

When $\omega = 0$, the $\langle \widehat{V} \rangle$ and $\langle \widehat{v} \dot{v} \rangle$ terms vanish as they are time derivatives of other quantities and therefore proportional to ω . It remains to calculate $\langle \widehat{V} \rangle$, $\langle \widehat{v}^2 \rangle$, and $\langle \dot{v}^2 \rangle$, and when $\omega = 0$ these can be calculated by taking the derivatives of the steady-state values with respect to $\bar{\alpha}_e$. Again, it is useful to use the shorthand $x_e = \tau_e / (\tau_v + \tau_e)$ and similarly for inhibition:

$$\lim_{\omega \rightarrow 0} \langle \widehat{v} h_e \rangle = \hat{\alpha}_e \tau_v \frac{\bar{\mathcal{E}}_e \kappa_e}{2\tau_e} x_e (1 - \bar{\alpha}_e \tau_v - \bar{\alpha}_e \tau_v x_e),$$

$$\lim_{\omega \rightarrow 0} \langle \widehat{v} h_i \rangle = -\hat{\alpha}_e \tau_v \frac{\kappa_i}{2\tau_i} \tau_v \bar{\alpha}_i x_i (\bar{\mathcal{E}}_e + \bar{\mathcal{E}}_i x_i). \quad (\text{C17})$$

For the low frequency limit of the variance modulation we break the response into excitatory and inhibitory components which take the form

$$\lim_{\omega \rightarrow 0} \langle \widehat{v}^2 \rangle^e = \hat{\alpha}_e \tau_v \frac{\bar{\mathcal{E}}_e^2 \kappa_e}{2} \frac{\tau_v}{\tau_e} x_e (1 - 3\bar{\alpha}_e \tau_v - \bar{\alpha}_e \tau_v x_e),$$

$$\lim_{\omega \rightarrow 0} \langle \widehat{v}^2 \rangle^i = -\hat{\alpha}_e \tau_v \frac{\kappa_i}{2} \frac{\tau_v}{\tau_i} x_i (2\bar{\mathcal{E}}_e \bar{\mathcal{E}}_i \tau_v \bar{\alpha}_i + \bar{\mathcal{E}}_i^2 \tau_v \bar{\alpha}_i + \bar{\mathcal{E}}_i^2 \bar{\alpha}_i \tau_v x_i).$$

Taking a similar approach with the variance of the rate-of-change of voltage gives

$$\begin{aligned}\lim_{\omega \rightarrow 0} \langle \widehat{v}^2 \rangle^e &= \hat{\alpha}_e \tau_v \frac{\bar{\mathcal{E}}_e^2 \kappa_e}{2\tau_e^2} x_e (1 - 2\bar{\alpha}_e \tau_v - \bar{\alpha}_e \tau_v x_e), \\ \lim_{\omega \rightarrow 0} \langle \widehat{v}^2 \rangle^i &= -\hat{\alpha}_e \tau_v \frac{\kappa_i}{2\tau_i^2} x_i (2\bar{\mathcal{E}}_e \bar{\mathcal{E}}_i \bar{\alpha}_i \tau_v + \bar{\mathcal{E}}_i^2 \bar{\alpha}_i \tau_v x_i).\end{aligned}$$

5. High-frequency asymptotics: isopotential model

For large ω , the leading-order contributions can be shown to decay as $1/\omega$ and comprise contributions from $\langle \widehat{V} \rangle$, $\langle \widehat{v} \widehat{v} \rangle$, and $\langle \widehat{v}^2 \rangle$. The forms for the first two are fairly straightforward to derive

$$\langle \widehat{V} \rangle \sim \frac{\hat{\alpha}_e \bar{\mathcal{E}}_e}{i\omega \tau_e} \quad \text{and} \quad \langle \widehat{v} \widehat{v} \rangle = -\frac{\hat{\alpha}_e}{i\omega \tau_e} \langle \widehat{v}^2 \rangle. \quad (\text{C18})$$

The third term is more complicated. We use

$$\langle \widehat{v} \widehat{h}_e \rangle = \bar{\mathcal{E}}_e \langle \widehat{h}_e^2 \rangle - \widehat{\mathcal{H}} \langle \widehat{v} \widehat{h}_e \rangle + \mathcal{O}\left(\frac{1}{\omega^2}\right), \quad (\text{C19})$$

and similar for $\langle \widehat{v} \widehat{h}_i \rangle$, though note that $\langle \widehat{h}_i^2 \rangle = 0$. Then

$$\langle \widehat{v}^2 \rangle = \bar{\mathcal{E}}_e \langle \widehat{v} \widehat{h}_e \rangle + \bar{\mathcal{E}}_i \langle \widehat{v} \widehat{h}_i \rangle - \widehat{\mathcal{H}} \langle \widehat{v} \widehat{v} \rangle + \mathcal{O}\left(\frac{1}{\omega^2}\right), \quad (\text{C20})$$

where for large ω we have

$$\langle \widehat{h}_e^2 \rangle \sim \frac{\hat{\alpha}_e \kappa_e}{i\omega \tau_e^2} \quad \text{and} \quad \widehat{\mathcal{H}} \sim \frac{\hat{\alpha}_e}{i\omega \tau_e}. \quad (\text{C21})$$

The quantities above can then be substituted into the linear response form of the upcrossing rate, which will therefore also have a $1/\omega$ behavior at high frequencies.

APPENDIX D: SIMULATIONS AND FIGURES

Simulation code was written using the Julia programming language [19] and all code used for figures is provided in the Supplemental Material [31]. The simulations were implemented using a forward Euler scheme typically with $\Delta_t = 0.02$ ms and $\Delta_x = 20$ μm so that

$$\begin{aligned}H_s(x_m, t_{n+1}) &= H_s(x_m, t_n) \\ &+ \frac{\Delta_t}{\tau_s} \left(\alpha_s(t_n) - H_s(x_m, t_n) \right. \\ &\left. + \sqrt{\alpha_s(t_n) \lambda_s} \frac{\phi_{mn}^s}{\sqrt{\Delta_x \Delta_t}} \right),\end{aligned} \quad (\text{D1})$$

and for the voltage

$$\begin{aligned}V(x_m, t_{n+1}) &= V(x_m, t_n) + \Delta_t (\alpha_\ell (E_\ell - V(x_m, t_n))) \\ &+ \Delta_t (H_e(x_m, t_n) (E_e - V(x_m, t_n))) \\ &+ \Delta_t (H_i(x_m, t_n) (E_i - V(x_m, t_n))) \\ &+ \frac{\Delta_t}{\Delta_x^2} D (V(x_{m-1}, t_n) - 2V(x_m, t_n) \\ &- V(x_{m+1}, t_n)),\end{aligned} \quad (\text{D2})$$

where ϕ_{mn}^s are independent Gaussian random numbers with zero mean and unit variance. The system was implemented

using periodic boundary conditions with size $L = 2000$ μm being sufficiently larger than spatial correlation lengths. Given the homogeneity of the system, statistical quantities such as the upcrossing could be evaluated at all positions simultaneously and averaged, thereby increasing the efficiency of the simulations.

For the isopotential neuron the discretization is across time only so the equations are

$$\begin{aligned}H_s(t_{n+1}) &= H_s(t_n) \\ &+ \frac{\Delta_t}{\tau_s} \left(\alpha_s(t_n) - H_s(t_n) + \sqrt{\alpha_s(t_n) \kappa_s} \frac{\phi_n^s}{\sqrt{\Delta_t}} \right),\end{aligned} \quad (\text{D3})$$

and for the voltage

$$\begin{aligned}V(t_{n+1}) &= V(t_n) + \Delta_t (\alpha_\ell (E_\ell - V(t_n))) \\ &+ \Delta_t (H_e(t_n) (E_e - V(t_n)) + H_i(t_n) (E_i - V(t_n))),\end{aligned} \quad (\text{D4})$$

where ϕ_n^s are again independent Gaussian random numbers with zero mean and unit variance.

Note that for both the dendritic and isopotential models, the schemes above can be straightforwardly modified to simulate the systems in the Gaussian approximation of the voltage in which terms that are second-order in zero-mean fluctuating quantities like $v h_e$ are dropped from the voltage dynamics.

1. The patterned input used in Fig. 2

The time-dependent input used in Fig. 2 comprised functions $\alpha_e(t)$ and $\alpha_i(t)$ lasting one second. Outside the range of 250 to 750 ms these rates were zero. Within this range both had constant value with $\bar{\alpha}_e = 0.00566$ kHz and $\bar{\alpha}_i = 0.01100$ kHz [which would give a constant upcrossing rate of 5 Hz, anticipating Fig. 3(c)] with the excitatory rate $\alpha_e(t)$ having four functions additionally superimposed. These functions $A(t)$ were parametrized as

$$A_k(t; a, t_k, \sigma, f_k) = a \exp\left(-\frac{(t - t_k)^2}{2\sigma^2}\right) \cos(2\pi f_k t), \quad (\text{D5})$$

where $a = 0.03$ kHz, $t_k = 350, 450, 550, 650$ ms, $\sigma = 20$ ms, and $f = 0.02, 0.05, 0.100, 0.200$ kHz.

2. Illustration of steady-state properties

Given the many components of the model, there is a broad choice of parameter combinations that might be used to illustrate behavior. In the context of examining the steady-state behavior [Figs. 3(b) and 3(c)] the choice was made to vary $\bar{\alpha}_e$ and $\bar{\alpha}_i$ at fixed ratio between τ_v and $\tau_\ell = 1/\alpha_\ell$ to give a particular $\langle \bar{V} \rangle$. Given the forms

$$\begin{aligned}\frac{1}{\tau_v} &= \alpha_\ell + \bar{\alpha}_e + \bar{\alpha}_i \quad \text{and} \\ \langle \bar{V} \rangle &= \tau_v (E_\ell \alpha_\ell + E_e \bar{\alpha}_e + E_i \bar{\alpha}_i),\end{aligned} \quad (\text{D6})$$

we therefore have the conditions

$$\begin{aligned}\bar{\alpha}_e &= \frac{(\langle \bar{V} \rangle - E_i) - (E_\ell - E_i)\alpha_\ell \tau_v}{(E_e - E_i)\tau_v} \text{ and} \\ \bar{\alpha}_i &= \frac{(E_e - \langle \bar{V} \rangle) - (E_e - E_\ell)\alpha_\ell \tau_v}{(E_e - E_i)\tau_v}.\end{aligned}\quad (\text{D7})$$

This parameter variation is used in Figs. 3(b) and 3(c).

3. Matching the isopotential and dendritic models

To provide as fair a comparison as possible between the models, we set the parameters of the isopotential model such that the steady-state mean voltage ($\langle \bar{V} \rangle$), conductance state τ_v ,

and voltage variance ($\overline{v^2}$) were all matched. The mean properties of the model are identical by design and set by $\bar{\alpha}_e$ and $\bar{\alpha}_i$. To match the variance, we choose κ_e and κ_i by comparing Eqs. (B8) and (C9) so that

$$\kappa_s = \frac{1}{2} \frac{\lambda_s}{\lambda_v} \left(\frac{\tau_v + \tau_s}{\tau_v} \right) \left(1 - \sqrt{\frac{\tau_s}{\tau_v + \tau_s}} \right). \quad (\text{D8})$$

Though the voltage mean and variance [Fig. 3(b), middle panel] as well as the conductance state parametrized by τ_v are matched, it is not possible [9] to simultaneously match the variance of the rate-of-change of voltage [see Fig. 3(b), lower panel] and so the upcrossing rates will not be the same; this can be seen in Fig. 3(c).

-
- [1] J. C. Magee, Dendritic integration of excitatory synaptic input, *Nat. Rev. Neuro.* **1**, 181 (2000).
- [2] N. Brunel, V. Hakim, and M. J. E. Richardson, Single neuron dynamics and computation, *Curr. Opin. Neurobio.* **25**, 149 (2014).
- [3] P. Poirazi and A. Papoutsis, Illuminating dendritic function with computational models, *Nat. Rev. Neuro.* **21**, 303 (2020).
- [4] H. C. Tuckwell and J. B. Walsh, Random currents through nerve membranes I. Uniform poisson or white noise current in one-dimensional cables, *Biol. Cybern.* **49**, 99 (1983).
- [5] A. Manwani and C. Koch, Detecting and estimating signals in noisy cable structures, II: Information theoretical analysis, *Neural Comput.* **11**, 1831 (1999).
- [6] H. C. Tuckwell, Spatial neuron model with two-parameter Ornstein-Uhlenbeck input current, *Physica A* **368**, 495 (2006).
- [7] H. C. Tuckwell, Computation of spiking activity for a stochastic spatial neuron model: Effects of spatial distribution of input on bimodality and CV of the ISI distribution, *Math. Biosci.* **207**, 246 (2007).
- [8] F. Aspart, J. Ladenbauer, and K. Obermayer, Extending integrate-and-fire model neurons to account for the effects of weak electric fields and input filtering mediated by the dendrite, *PLoS Comput. Biol.* **12**, e1005206 (2016).
- [9] R. P. Gowers, Y. Timofeeva, and M. J. E. Richardson, Low-rate firing limit for neurons with axon, soma and dendrites driven by spatially distributed stochastic synapses, *PLoS Comput. Biol.* **16**, e1007175 (2020).
- [10] S. O. Rice, Mathematical analysis of random noise, *Bell. Syst. Tech. J.* **24**, 46 (1945).
- [11] P. Jung, Stochastic resonance and optimal design of threshold detectors, *Phys. Lett. A* **207**, 93 (1995).
- [12] T. Verechtchaguina, I. M. Sokolov, and L. Schimansky-Geier, First passage time densities in resonate-and-fire models, *Phys. Rev. E* **73**, 031108 (2006).
- [13] Y. Burak, S. Lewallen, and H. Sompolinsky, Stimulus-dependent correlations in threshold-crossing spiking neurons, *Neural Comput.* **21**, 2269 (2009).
- [14] T. Tchumatchenko, A. Malyshev, T. Geisel, M. Volgushev, and F. Wolf, Correlations and Synchrony in Threshold Neuron Models, *Phys. Rev. Lett.* **104**, 058102 (2010).
- [15] L. Badel, Firing statistics and correlations in spiking neurons: A level-crossing approach, *Phys. Rev. E* **84**, 041919 (2011).
- [16] J. R. León and A. Samson, Hypoelliptic stochastic FitzHugh-Nagumo neuronal model: Mixing, up-crossing and estimation of the spike rate, *Ann. Appl. Probab.* **28**, 2243 (2018).
- [17] T. Schwalger, Firing statistics and correlations in spiking neurons: A level-crossing approach, *Biol. Cybern.* **115**, 539 (2021).
- [18] A. Sanzeni, M. H. Histed, and N. Brunel, Emergence of Irregular Activity in Networks of Strongly Coupled Conductance-Based Neurons, *Phys. Rev. X* **12**, 011044 (2022).
- [19] J. Bezanson, A. Edelman, S. Karpinski, and V. B. Shah, Julia: A fresh approach to numerical computing, *SIAM Rev.* **59**, 65 (2017).
- [20] M. J. E. Richardson and W. Gerstner, Synaptic shot noise and conductance fluctuations affect the membrane voltage with equal significance, *Neural Comput.* **17**, 923 (2005).
- [21] C. Koch, Cable theory in neurons with active, linearized membranes, *Biol. Cybern.* **50**, 15 (1984).
- [22] S. Coombes *et al.*, Branching dendrites with resonant membrane: a “sum-over-trips” approach, *Biol. Cybern.* **97**, 137 (2007).
- [23] F. Droste and B. Lindner, Exact analytical results for integrate-and-fire neurons driven by excitatory shot noise, *J. Comput. Neurosci.* **43**, 81 (2017).
- [24] M. J. E. Richardson, Spike shape and synaptic-amplitude distribution interact to set the high-frequency firing-rate response of neuronal populations, *Phys. Rev. E* **98**, 042405 (2018).
- [25] N. Fourcaud-Trocmé and N. Brunel, How spike generation mechanisms determine the neuronal response to fluctuating inputs, *J. Comput. Neurosci.* **18**, 311 (2005).
- [26] B. Naundorf, F. Wolf, and M. Volgushev, Unique features of action potential initiation in cortical neurons, *Nature* **440**, 1060 (2006).
- [27] V. Ilin, A. Malyshev, F. Wolf, and M. Volgushev, Fast computations in cortical ensembles require rapid initiation of action potentials, *J. Neurosci.* **33**, 2281 (2013).
- [28] G. Eyal *et al.*, Dendrites impact the encoding capabilities of the axon, *J. Neurosci.* **34**, 8063 (2014).

- [29] S. Ostojic, G. Szapiro, E. Schwartz, B. Barbour, N. Brunel, and V. Hakim, Neuronal morphology generates high-frequency firing resonance, *J. Neurosci.* **35**, 7056 (2015).
- [30] J. Dose and B. Lindner, Noisy juxtacellular stimulation in vivo leads to reliable spiking and reveals high-frequency coding in single neurons, *Phys. Rev. E* **96**, 032109 (2017).
- [31] See Supplemental Material at <http://link.aps.org/supplemental/10.1103/PhysRevResearch.5.023095> for computer code used to generate Figs. 1, 2, and 3.